ELSEVIER

Contents lists available at ScienceDirect

Results in Engineering

journal homepage: www.sciencedirect.com/journal/results-in-engineering





Maximum grid spacing effect on peak pressure computation using inflow turbulence generators

Zahra Mansouri ^a, Rathinam Panneer Selvam ^{a,*}, Arindam Gan Chowdhury ^b

- ^a BELL 4190, University of Arkansas, Fayetteville, AR, 72701, USA
- ^b Florida International University, Miami, FL, USA

ARTICLE INFO

Keywords:
Computational fluid dynamics
Synthetic inflow turbulence
Peak pressure
TTU building
Large eddy simulation

ABSTRACT

The peak pressures are computed using computational fluid dynamics (CFD) with the synthetic inflow turbulence generator and compared with 1:6 scale Texas Tech University (TTU) wind tunnel measurements. The inflow turbulence is calculated using the Consistent Discrete Random Flow Generation Method (CDRFG) method. The maximum and minimum frequencies from the field or experimental measurements as input to the inflow turbulence generator without considering the largest grid spacing used in the CFD model leads to high pressure error. For one case, more than 100% error in peak pressure results is observed. In addition, spurious pressures are observed at the building location without building. By varying maximum frequencies systematically for each computational mesh size and comparing the velocities and pressures at the inflow and the building location without building, possible causes of the error are explained. From the investigation, it is suggested not to use the maximum frequency in the inflow turbulence generator beyond the frequency that can be transported by the largest grid spacing.

1. Introduction

Significant infrastructure damage, economic loss, and even deaths are caused by severe windstorms such as hurricanes and tornadoes. The National Weather Service (NWS) reported 38 fatalities, 202 injured, and damages resulting in costs of 187.67 million dollars caused by severe thunderstorm wind in 2019 [1]. Based on this report, the number of fatalities and costs of structural failures increased by 14 people and 31.81 million dollars in 2019 compared to 2018. Because wind flows have higher intensity currently compared to the past, and it is expected to increase more in the future [2]. Hence, a better estimation of wind peak pressures and loads on buildings is required to design structures. As an illustration, for component and cladding, the maximum peak pressure coefficient (Cp) obtained from ASCE 7-16 is -3.2 for a low-rise building. However, field measurements have reported that the maximum peak Cp on a low-rise building can be lower than -8 [3]. As conducting field measurement is time-consuming and costly to estimate wind loads on structures, computational fluid dynamic (CFD) can be used as an economical alternative tool. With the cutting-edge improvements in the CFD, the possibility of computing peak pressures is very near. A well-validated CFD with field measurements can fill this gap and help to reduce the loss of damage and loss of life.

As strong winds are highly turbulent, turbulence needs to be well accounted for in CFD. The turbulence's effects in wind can be incorporated in CFD by using various turbulence modeling methods. Large Eddy Simulation (LES) is more reliable and applicable in the industry compared to all other turbulence modeling methods. However, a critical aspect of the numerical LES investigation is defining the right inflow turbulence condition to predict peak pressure correctly. Selvam [4] reported at least 30% error in CFD peak *Cp* compared to field measurements is rooted in low grid resolution and inflow boundary conditions (BC). Primary methods to generate inflow turbulence fields are (a) precursor database, (b) recycling method, and (c) synthetic turbulence [5]. The weakness of the first method is the need for the precursor database that makes this method computationally expensive. The second method is not practical because it is computationally costly and is sensitive to roughness.

1.1. Peak pressure on low-rise buildings' estimation status using synthetic inflow methods

As synthetic inflow turbulence does not require prior flow

E-mail addresses: zmansour@uark.edu (Z. Mansouri), rps@uark.edu (R.P. Selvam), chowdhur@fiu.edu (A.G. Chowdhury).

^{*} Corresponding author.

simulations, recent studies used it as a preferable method [6–9]. In these studies, the time-varying pressures on buildings due to different synthetic turbulent inflows are reviewed and not mentioned here. Numerous synthetic inflow turbulence methods are in use and can be categorized into (1) Random Flow Generation method (RFG), (2) Digital Filtering Method (DFM), and (3) Synthetic Eddy Method (SEM). In all the mentioned references, improved RFG methods are used to compute flow around the Commonwealth Aeronautical Advisory Research Council (CAARC) standard tall building. For instance, Aboshosha et al. [7] developed and used the 4th generation of RFG methods (i.e., Consistent Discrete Random Flow Generation (CDRFG)) to compute peak pressure on tall buildings. Whereas Aboshosha et al. [7] used two terms in their Fourier series, Yu et al. [9] used one term to reduce the computation time of inflow generation by at least 5 times. As examples for other synthetic methods, Daniels et al. [10] used the modified DFM by Kim et al. [11] for the CAARC standard tall building, and Poletto et al. [12] used SEM for channel flow.

However, in the works of Daniels et al. [10], Aboshosha et al. [7], and Yu et al. [9], the root-mean-square (RMS) and the mean pressure coefficients for the CAARC tall building are compared with wind tunnel (WT) results, and results are very encouraging. Daniels et al. [10] focused on the surface pressures correlation with WT results comparison. Hence, there is no comparison of CFD peak pressure with WT or field measurements for a low-rise building, and the current work focuses on that. In this work, to improve the predictive capability of low-rise building damages, the Texas Tech University (TTU) building is considered as a benchmark problem. Wind tunnel measurements of peak pressures on the TTU building are provided by Moravej [13]. Furthermore, the inflow turbulence field is calculated using CDRFG. In addition to the CDRFG method, the other RFG method used in our group is Narrowband Synthesis Random Flow Generator (NSRFG) method introduced by Yu et al. [9]. The NSRFG method's results are provided by Atencio [30] and Selvam [31], and in this study, only the results related to CDRFG are presented. The MATLAB code for the CDRFG method is provided in the appendix by Aboshosha et al. [7]. The verification and validation of the model are reported in detail by Aboshosha et al. [7].

2. Relation between maximum grid spacing and the maximum possible frequency

Turbulent flow includes some circular movement of fluid called eddies. In a typical turbulent flow, there exists a wide range of eddy sizes fluctuating at different frequencies (i.e., large eddies have large velocity fluctuations of low frequency and vice versa). To capture each addy in LES, minimum four CFD mesh is required as shown in Fig. 1(a). Mesh can resolve different sizes of eddies as shown in Fig. 1(b). As each eddy fluctuates at a specific frequency, hence, only a certain range of frequency can be transported by a specific maximum grid spacing in LES [21,22]. The largest frequency that a grid can resolve is called f_{LES} as shown in Fig. 2. Additionally, to avoid LES filtering effects, the filter length (Δ) is considered equal to grid spacing size (h) (i.e., $\Delta/h=1$) in the current LES modeling. Hence, eddies with the wavelength (L) smaller than filter length (Δ) which equals to mesh size here (i.e., Fig. 1 (c)) cannot be resolved and are modeled by a sub-grid scale model such as Smagorinsky model. In Fig. 2, the non-dimensional maximum and

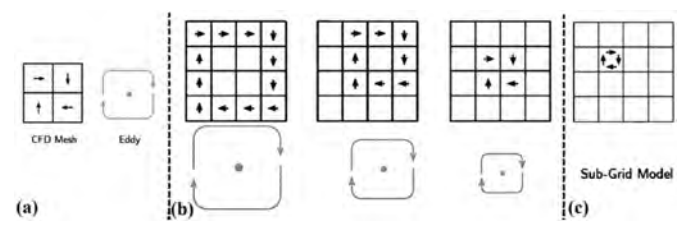


Fig. 1. Different eddy sizes compared to the mesh size.

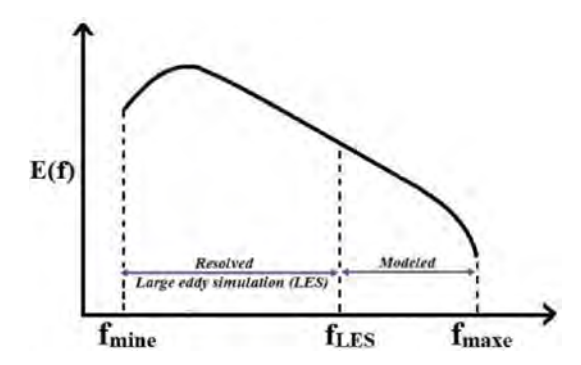


Fig. 2. Frequency region resolved and modeled by LES.

minimum frequency from field measurements or WT is referred to f_{maxe} and f_{mine} . Furthermore, the non-dimensional maximum frequency (f_{max}) used as input to the inflow turbulence models is referred to f_{max} and the minimum one is f_{min} .

For a specific grid spacing of h, the minimum wavelength L of a wave in the form of sine or cosine function transported by the Fourier spectral method is 2h [17]. The corresponding frequency is called the Nyquist frequency in the spectral analysis. Even though transport of Nyquist frequency is possible with the spectral method, the amount of error using the finite difference method (FDM) is very high. Consequently, to have fewer errors, Ferziger and Peric [18] and Kravchenko and Moni [19] suggested L=4h for finite difference or control volume method, which its corresponding frequency is f_{grid} . Even to have more than 90% accuracy, Selvam [20] recommended using L=10h, but this level of the refined grid is not practical. An example of transporting a sine wave with the wavelength of 2h and 4h is provided in appendix B to understand it. In the appendix B, the error of transporting of a sine wave with the wavelength of 2h is shown around 100%, which is not acceptable. For the wavelength of 4h, it is around 25%.

As discussed, the highest frequency that can be transported by the grid will be f_{grid} and it equals f_{LES} in the LES studies. As a result, with a reasonable error, L=4h can transport a wave with the frequency of n_{LES} and the corresponding non-dimensional frequency of fLES. fLES in terms of L is calculated by Eq. (1) as the relation between frequency and wavelength is $L=U_H/n$.

$$f = \frac{1}{\lambda} = \frac{H}{L} = \frac{nH}{U_H} \tag{1}$$

where λ is the non-dimensional wavelength, H is the building height, and U_H is the mean velocity at the building height. Hence, the suggested highest non-dimensional frequency transported in the flow using the FDM and LES is calculated as $f_{LES} = f_{grid} = H/4h$ using Eqn. (1). As an example, for L=4h and h=H/16 grid, f_{LES} is calculated as $f_{LES}=H/(4H/16)=4$. Rana et al. [23] reported that the inflow turbulence using Digital Filter Method (DFM) dissipate immediately in the computational domain because the energy is not distributed over the required range of frequencies. Similarly, Kokkinos's et al. [24] tried to budget energy to low-frequency to reduce the numerical dissipation of the scheme and thus improve the accuracy of the results, particularly for under-resolved grids. Hence, this study tries to present the effect of choosing frequency beyond f_{LES} on peak pressure results.

3. Definition of spurious pressure

Rigall et al. [14], Haywood [15] and Lebovitz [16] reported that spurious pressure occurs due to many of the inflow turbulence generator methods. Rigall et al. [14] used the adapted RFG method and Lebovitz [16] used DFM. In all these works, the mentioned spurious pressure happens when the pressure frequency is higher than the velocity frequency. As an example, when the inflow turbulence field is calculated

using CDRFG for the f_{max} = 10 and the grid spacing of h = H/16, the Nyquist frequency is H/2h = H/2(H/16) = 8 for this grid. In Fig. 3, the pressure is plotted at the inlet and building location for this case. If frequencies are taken as the number of peaks or cycles per unit time, the pressure frequency is about 9–10. As velocity frequency cannot be higher than Nyquist frequency, spurious pressures are pressures that have frequencies higher than the Nyquist frequency in this study. Hence, the above-mentioned case has spurious pressures.

It should be noted that previous researchers identified pressure fluctuation and stated some reasons for these unwanted pressures. As an example, if an inflow does not preserve momentum for each spatial direction (i.e., does not respect the Taylor hypothesis) or does not respect mass conservation (i.e, being divergence-free), produces unwanted pressure fluctuations as explained by Patruno and Ricci [6]. In addition to mentioned reasons, boundary condition mismatches leads to unwanted pressure productions near boundaries as explained in detail by Patruno and Ricci [25]. Patruno and Miranda [26] developed a method to mitigate unwanted pressures created due to violation of divergence free condition and Taylor hypothesis. However, they used only a sinewave that respects LES frequency and wavenumber and they stated pressure fluctuation decreases after a distance from the inlet (Fig. 4). Whereas, what is declined is the amplitude of pressure fluctuation and not its frequency (Fig. 3). In Fig. 3, pressure is plotted at the building height at the inlet and the building location. As it can be seen in this figure, the amplitude of pressure decreases at the building location compared to the inlet location. However, the frequency of pressure remains unchanged. Mansouri et al. [27] showed similar issues using other methods such as the digital filter method.

4. Objectives

Generally, $f_{max} = f_{maxe}$ and $f_{min} = f_{mine}$ are used as input to inflow turbulence generators regardless of the CFD grid size.

- 1. To understand the effect of various f_{max} on spurious pressures, CFD model without building is considered for f_{max} of f_{maxe} and f_{LES} for the grid spacing of H/16, and then the pressure coefficient over time is plotted at the building location.
- 2. To show the effects of spurious pressure on peak pressures, CFD model with building is considered. First, the peak pressures on the 1:6 scale TTU building are calculated for f_{max} equal to f_{maxe} and f_{LES} for various grid spacing (i.e., H/8, H/16, and H/24). These results are compared with the WT and field measurements results reported by Moravej [13]. Since the finest grid leads to 8.62 million grid points,

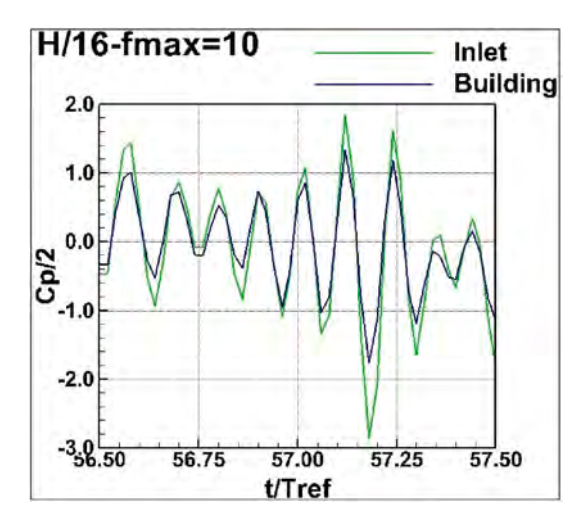


Fig. 3. Non-dimensional velocity at the inlet and the building location and pressures coefficient at the building location without building for h=H/16, $f_{max}=10$, and for 1 time unit.

we did not go for further refinements, and H/16 are chosen to use for investigating the effect of f_{max} used in the inflow turbulence model on peak pressures. The f_{max} in the CDRFG is varied from less than f_{LES} to f_{max} .

Finally, based on the analysis of the above work, a proper procedure to use the synthetic turbulence method to calculate peak pressures with less error is proposed.

5. Numerical setup

5.1. Computer modeling and boundary conditions

The 3D incompressible Navier–Stokes (NS) equations are used for flow computations, and Large Eddy Simulation (LES) with Smagorinsky one equation model is used for turbulence modeling. The three-dimensional equations for an incompressible fluid using LES model in general tensor notation are as follows:

Continuity equation
$$U_{i,i} = 0$$
. (2)

Momentum equation:
$$U_{i,t} + U_j U_{i,j} = -(p/\rho + 2k/3)_{,i} + [(\nu + \nu_t)(U_{i,j} + U_{j,i})]_{,i}$$
 (3)

where, $\nu_t = (C_s h)^2 (S_{ij}^2/2)^{0.5}$, $S_{ij} = U_{i,j} + U_{j,i}$, $h = (h_1 h_2 h_3)^{0.333}$ for 3D, and $k = (\nu_t/(C_k h))^2$; empirical constants are $C_s = 0.1$, and $C_k = 0.094$.

The details of the equations and the solution procedure for the NS equation based on the fractional step are reported by Selvam [4]. The variables in the NS equations are approximated by the central difference method. A non-staggered grid system is used. The variables in time are approximated by the Crank-Nicolson method. The momentum equations are solved by line iteration, and pressure equations are solved by preconditioned conjugate gradient (PCG) method. The PCG algorithmic details are provided in Selvam [28]. A maximum sub-iteration of 10 is used in addition to reducing the error for required convergence in momentum and continuity equations at each time step. Hence, the errors in all the equations are eliminated. The NS equations are non-dimensionalized using the building height (H) and the average velocity at the building height (U_H) as the reference values. The corresponding reference time (T_{ref}) is calculated as H/U_H . The roughness length (z_0) is 0.05 m.

The uniform grid spacing of H/8, H/16, and H/24 (where H is the building height of the TTU building) in all directions are considered in the current study. The domain size used for computation is $13.3H \times$ $9.375H \times 5H$, and the location of the building within the computational domain is shown in Fig. 5. The grid size equals $213 \times 151 \times 81$ with 2,605,203 nodes for H/16 grid spacing and $319 \times 226 \times 121$ with 8,723,374 nodes for H/24 grid spacing. The building is located at 4Hfrom the inflow. The dimension of the TTU building is $2.25H \times 3.375H \times$ H, where H is 3.96 m. The flow is considered to be along with the shorter length (2.25H) of the TTU building. Although CFL (Courant-Friedrichs-Lewy) can be greater than 1.0 because of using implicit solvers, the CFL criterion is kept less than 1.0 to capture all the time-variant issues. The maximum velocity around the building is approximately $2U_H$ based on the computation: thus. the $dt = dX/U_{max} = (H/16)/2U_H = 0.03125(H/U_H)$ the or dimensional time step dt should be less than 0.03125 to preserve CFL < 1.0. In this study, a non-dimensional time step of dt = 0.02 is used, and the corresponding CFL is equal to 0.64. The computation is conducted for 100 non-dimensional time units (5000 time steps for H/16grid). The Reynolds number (Re = HU_H/ν) used in the CFD model is 2.5 \times 10⁶. The Re is calculated based on the full-scale dimensions reported in Table 1.

The boundary conditions are indicated for all surfaces in Fig. 5. The symmetric boundary conditions are implemented on the sidewalls, and the outflow boundary condition is specified at the outlet. On the wall, no

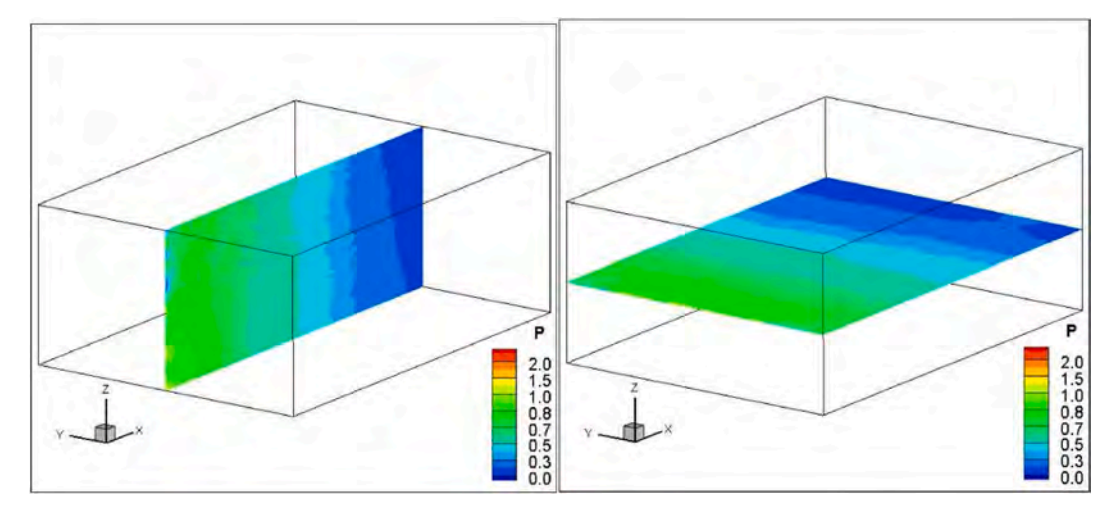


Fig. 4. Pressures coefficient contour without building for h = H/16, $f_{max} = 10$.

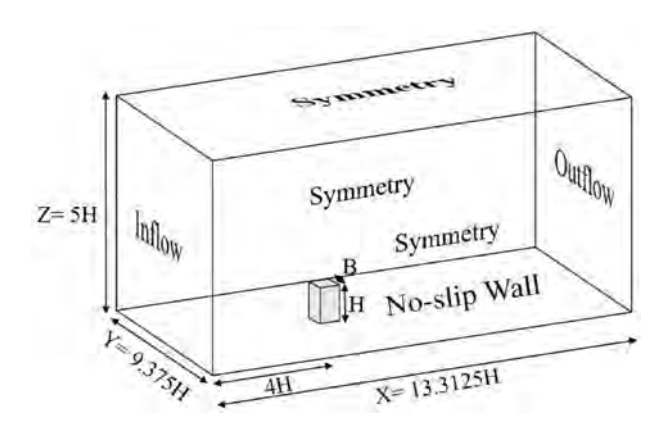


Fig. 5. Boundary conditions for the numerical modeling.

slip with the law of the wall condition is implemented. At the inflow, the calculated velocities using the CDRFG method are applied at each time step. The details of the inflow velocity computation are described in section 5.2. The CDRFG method calculates velocity field as follows:

$$u_i(x_j,t) = \sum_{m=1}^{M} \sum_{n=1}^{N} p_i^{m,n} \cos\left(k_j^{m,n} x_j^m + 2\pi f_{m,n}t\right) + q_i^{m,n} \sin\left(k_j^{m,n} x_j^m + 2\pi f_{m,n}t\right)$$
(4

In this equation, x_j^m are non-dimensionalized coordinates by dividing real coordinates x_j to $L_j^m = U_{ave}/\gamma C_j f_m$, , and $k_j^{m,n}$ are coordinates of uniformly distributed points on a unit radius sphere that satisfy the divergence-free condition in the CDRFG method. Details for calculation constants (i.e., C_j and γ) and amplitudes (i.e., $p_i^{m,n}$ and $q_i^{m,n}$) based on the wind spectrum are provided by Aboshosha et al. [7].

5.2. The inflow turbulence computation details

The input data details for the CDRFG MATLAB program are provided by Aboshosha et al. [7]. The velocity at the inflow is computed for the actual TTU building and then the velocity is scaled to non-dimensional value via dividing by U_H . The considered turbulent characteristics in the field indicated in Table 1 are derived from Mooneghi et al. [3]. The turbulent spectra equations used for the three velocities and the coherence functions used are reported in detail by Aboshosha et al. [7] and they are not repeated here. An analytical equation for the WT spectra is not available for the 1:6 scale study and so we used the von Karman spectra until the peak values of the WT spectra match with the

Table 1Turbulent characteristics for the TTU building [3.7]

Turbulent characteristics for the 110 building [3,/]	
Parameters	Full-Scale Model
Reference height	H=3.96m
Reference wind velocity	$U_H = 7.66 \ m/s$
Mean velocity	$U_{ave} = U_H \left(\frac{z}{H}\right)^{\alpha} m/s, \ \alpha = 0.326$
Turbulence Length scale	$L_j = L_{jH} \left(rac{z}{H} ight)^{dLj}, \ m j = u, v, w$
	$L_{uH} = 0.302 m, L_{vH} = 0.0815 m, L_{wH} =$
	0.0326 m
	$dL_u = 0.473, dL_v = 0.881, dL_w = 1.539$
Turbulent intensity I	$I_j = I_{jH} ig(rac{z}{H}ig)^{-dj}, j = u, \ v, \ w$
	$I_{uH} = 0.216, I_{vH} = 0.207, I_{wH} = 0.120$
	$d_u = 0.191, d_v = 0.123, d_w = 0.005$
Minimum frequency	$n_{min} = 0.19 (Hz)$
	$f_{min}=0.1$
Maximum frequency	$n_{max} = 1.93, 3.9, 5.8, 7.74, 15.44, and 19.$ 23 (Hz)
	$f_{max} = 1, 2, 3, 4, 8, and 10$
number of time step	5000 for <i>H</i> /8 & <i>H</i> /16 grid and 10,000 for <i>H</i> /24
Time step	dT = 0.0103 s for $H/8 & H/16$ and 0.005 s
	for <i>H</i> /24
	dt = 0.02 units for $H/8$ & $H/16$ and
	0.00965 units for H/24
M, Number of frequency segments	100
N, Number of random frequencies	100
in one segment	
Frequency steps	$\Delta n = \left(\frac{n_{max} - n_{min}}{M - 1}\right) = 0.02, 0.04, 0.06, 0.08,$
	0.15,&0.19(Hz)
	$\Delta f = \left(\frac{f_{max} - f_{min}}{M - 1}\right) = 0.01, 0.02, 0.03, 0.04,$
	0.08,&0.1

von Karman spectra. Since the verification and validation were conducted in the above reference using the MATLAB code, this work focuses mainly on the effects of spurious pressure error and high-frequency wind at the inflow on peak pressures on the building.

The f_{min} is kept at a constant value of $f_{mine} = 0.1$. The f_{max} varies for different grids. If $f_{max} = f_{LES}$ is kept as per section 2, then for H/8, H/16, and H/24 grid the f_{max} comes to be 2, 4, and 6 respectively. The different f_{max} used in the CFD calculations are between $f_{max} < f_{LES}$ and $f_{max} = f_{max}$ frequencies are 1,2,3, 4, 8, and 10. The dimensional frequency n_{max} can be calculated knowing f_{max} using Eq. (1). As an example, for $f_{max} = 10$, $n_{max} = f_{max}U_H/H = 10 \times 7.66/3.96 = 19.34$ Hz. Similarly, other ones can be converted to dimensional ones and are reported in Table 1. Aboshosha et al. [7] calculated the number of frequency segments (i.e.,

M) of 50 using the formula $M=f_{max}/2f_{min}$ for $f_{max}=10$ and $f_{min}=0.1$. They used random frequencies number N in one segment (i.e., N) as 100. In the current study, N has kept the same value of 100, and M is kept 100 for all cases. The dimensional time step (dT) used in the CDRFG is calculated knowing the non-dimensional time step of dt=0.02 for H/16 and H/8 grid as follows:

$$dt = \frac{dT}{T_{ref}} = > dT = dt \times T_{ref} = dt \times \frac{H}{U_H} = 0.02 \times \frac{3.96}{7.66} = 0.0103$$
 (5)

The CDRFG program is run using the above-mentioned initial data, and the velocities at the inlet are stored for 5000 time steps or 100 non-dimensional time units for H/8 and H/16 grid and 10,000 time steps for H/24 grid. The produced dimensional velocities from CDRFG are converted to the non-dimensional ones via dividing the velocities by U_H . Then, these inlet velocities are read from the input file at each time step. The initial conditions in the computational domain for velocities are provided as mean velocities.

5.3. Wind tunnel test detail

In the 1:6 scale WT study conducted by Mooneghi et al. [3] and Moravej [13], the TTU building model height was 0.66 m and the mean wind speed at the building height was 19.48 m/s. For this large-scale testing, the Re was 8.6×10^5 , which is much closer to the field Re of 2.5×10^6 , compared to that in any other WT study in the literature. The wind spectrum from the WT study was compared with the Von Karman spectrum in Moravej [13]. The discrepancy of the 1:6 WT spectrum with respect to the Von Karman spectrum in the low-frequency range (f < 0.1) is explained in detail. The local pressures on the building were measured using 204 pressure taps. The pressure taps were located exactly at the same location as in the field measurements for allowing meaningful comparison. The pressure coefficients were measured and reported for various wind directions with respect to the building (0°-360°, at an increment of 3°). In this study, only the 90° wind direction range is considered for comparison with CFD computation. Further details on the WT study can be found in Moravej [13].

6. Results and discussions

The CDRFG method is chosen to investigate the effects of maximum frequency on the mentioned spurious pressure. Afterward, the effects of maximum frequency regarding different grid spacing sizes on the peak and mean pressure coefficients are investigated.

To validate the CDRFG method, the time-averaged velocity is calculated and compared with the targeted mean velocity profile for the grid spacing size of H/16 and $f_{max}=10$ (Fig. 6(a)). According to this figure, there is not any difference between the targeted and the calculated mean velocity profile. Furthermore, the velocity spectrum is

plotted at the inlet and compared with the Von Karman spectrum (Fig. 6 (b)). Likewise, a reasonable correlation exists between the CDRFG velocity spectrum and the Von Karman spectrum.

6.1. Effects of $f > f_{LES}$ on spurious pressure at the building location

According to Fig. 7, pressure over time is plotted for $f_{max}=10$ and $f_{max}=f_{LES}=4$ for the grid spacing size of H/16, on way to investigate the effects of maximum frequency on spurious pressures. In Fig. 7 (c) and (d), the pressure variation has the frequency of 10 and 7 respectively for $f_{max}=10$ and $f_{max}=f_{LES}=4$ at the building location. Hence, as f_{max} decreases from 10 to f_{LES} , the frequency of pressure variation at the building location decreases to less than Nyquist frequency. Consequently, it seems the error of grid resolution considerably influences the spurious pressure fluctuations.

6.2. Effect of spurious pressure on the peak pressure results

To investigate the effects of spurious pressure existence on the pressure results, the peak pressure is firstly compared with WT and field pressure measurements for different grid sizes at $f_{max}=10$ and $f_{max}=f_{LES}$. To calculate the peak pressure, the following procedure is used. Generally, about 10 time units are needed for the turbulent flow to be fully developed and hence it is ignored. The remaining data from 10 time units to 100 time units are considered to capture the peak pressures at each point in time. Then, the peak pressure results will be compared with WT pressure measurements for different f_{max} for the grid size of H/16. Finally, it will be shown that the mean pressure result as an evaluation option is not reliable.

6.2.1. Comparison of minimum and maximum peak pressures for various grid size spacing for $f_{max}=10$ and Grid's f_{LES} with WT and field measurements

In the LES computation, the grid spacing h determines the f_{max} used as we discussed in detail before. Hence, for different grid spacing, different $f_{max}=f_{LES}$ are used in Fig. 8(d)–(f). To compare the current procedure of using $f_{max}=10$ and $f_{max}=f_{LES}$, the minimum pressure coefficient C_{pmin} is reported in Fig. 8 for 3 different grid sizes (H/8, H/16 and H/24). The top figures are for $f_{max}=10$ and the bottom figures are $f_{max}=f_{LES}$. From left to right the grid is refined. One can see the high error for $f_{max}=10$ in Fig. 8(a)–(c). The pressure coefficients are approaching the WT values from higher absolute value for $f_{max}=10$ case as in Fig. 8(a)–(c) and from lower absolute value for $f_{max}=f_{LES}$ case as in Fig. 8(d)–(f). The $f_{max}=f_{LES}$ case is similar to solid mechanics grid convergence studies. The high error in H/8 grid in Fig. 8(d) may be due to not having the necessary grid resolution as well as violating the isotropic assumption of the LES. So, systematic convergence due to grid refinements are observed in Fig. 8(e)–(f) using $f_{max}=f_{LES}$ more clearly

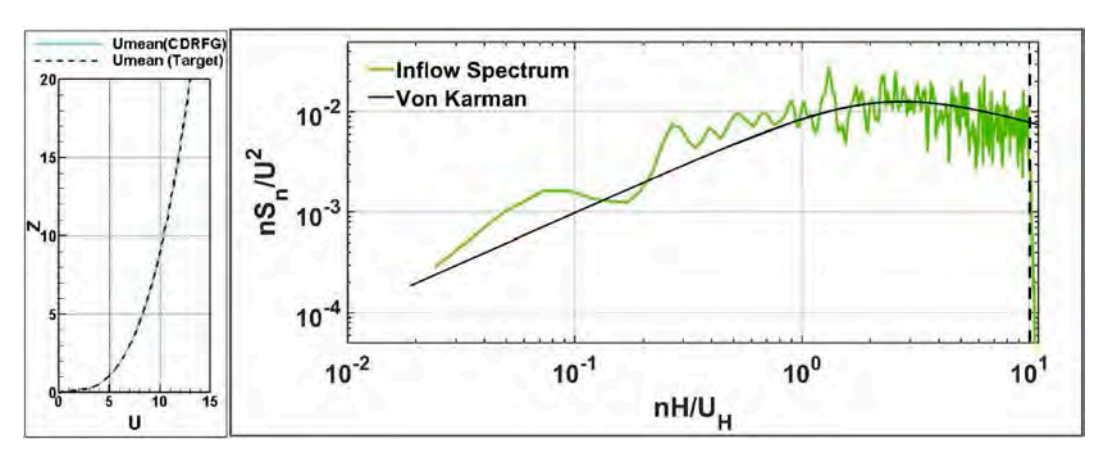


Fig. 6. Comparing a) the CDRFG mean velocity profile to the targeted one and b) the inlet velocity spectrum to the Von Karman spectrum.

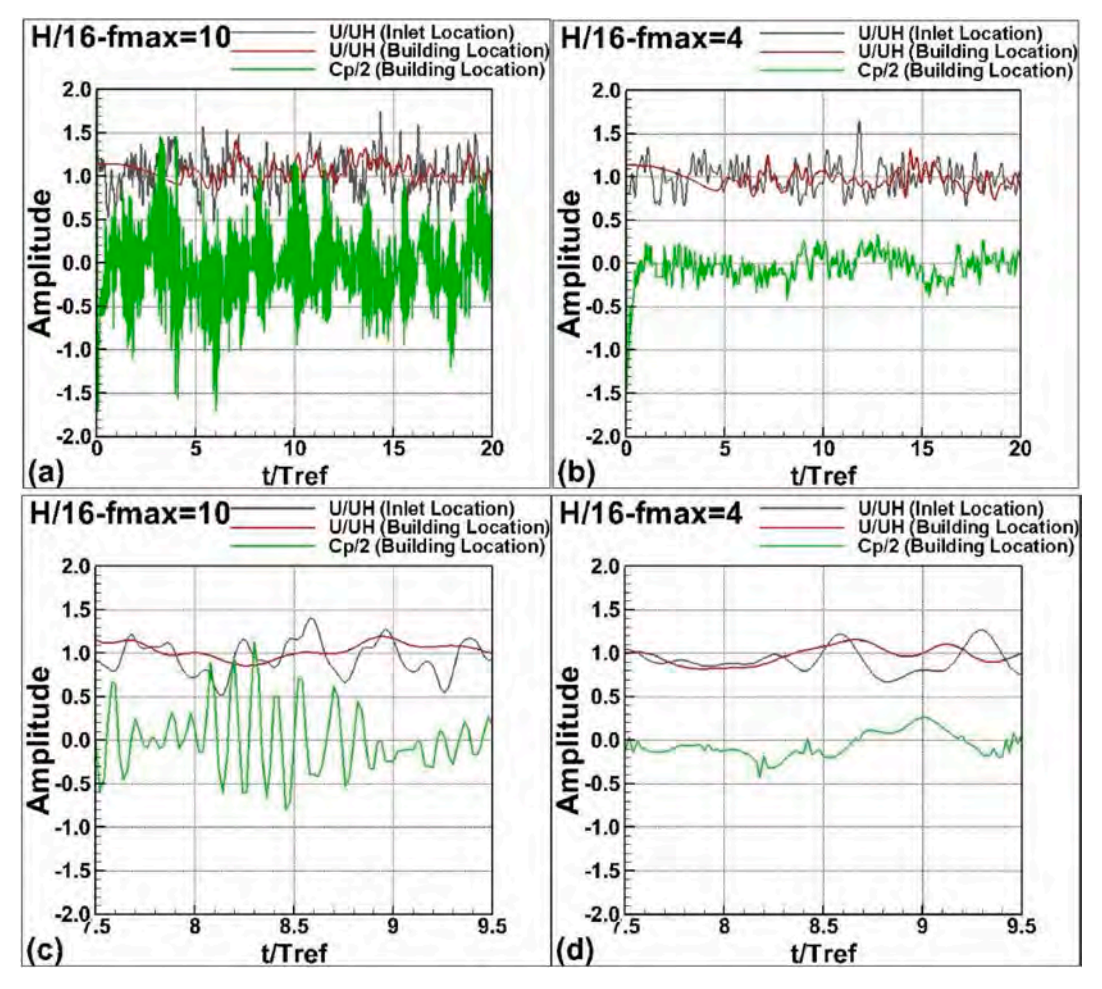


Fig. 7. Non-dimensional velocity at the inlet and at the building location and pressures coefficient at the building location without building for h = H/16 (a) $f_{max} = 10$ (b) $f_{max} = 4$ (c) $f_{max} = 10$ close up to 2 time units (d) $f_{max} = 4$ close up to 2 time units.

than in Fig. 8(a)–(c) using $f_{max}=10$. In Fig. 8(a), for not having proper grid refinement C_{pmin} should be less than the WT and field measurement but shows the other way because of numerical error, spurious pressure error, and other errors before. The roof error is reduced and the C_{pmin} is much close to WT and field measurements when $f_{max}=f_{LES}$ but the windward and leeward errors are high even for the case of $f_{max}=f_{LES}$. From Fig. 8(d)–(f) one can also see that H/16 grid C_{pmin} values are close to H/24 grid and this is the reason H/16 grid is considered for many comparisons in the next sections. If $f_{max}=f_{grid}=f_{LES}>10$, then some of the numerical errors mentioned in Fig. 8(a)–(c) could be avoided automatically but with extensive computer storage and computer time. The H/24 grid took close to 8 days whereas H/16 grid took about a day for each computation.

Similarly, to compare the current procedure of using $f_{max}=10$ with $f_{max}=f_{LES}$, the maximum pressure coefficients C_{pmax} are plotted in Fig. 9 for 3 different grid sizes (H/8, H/16 and H/24). The top figures are for $f_{max}=10$ and the bottom figures are $f_{max}=f_{LES}$. From left to right the grid is refined. One can see the high error for $f_{max}=10$ in Fig. 9(a)–(c). In Fig. 9(f) for H/24 grid, the maximum peak pressure coefficient is in much better agreement with field data than H/16 and H/8 grids. In Fig. 9(d)–(f) also one can see that on the windward wall the error is less for H/8 grid than H/16. For computing negative pressure H/8 grid is not sufficient.

6.2.2. Comparison of minimum and maximum peak pressures for various f_{max} with WT

To evaluate that f_{LES} is chosen correctly, the minimum peak pressure coefficients C_{pmin} for the six f_{max} cases are plotted in Fig. 10 for H/16

grid. The minimum values are calculated using the same 10 time units to 100 time units data. The CFD peak pressures are compared with WT6 and field data. The error on the roof is very high for $f_{max}=10$ (Fig. 10 (a)), and as f_{max} decreases, the error decreases systematically (Fig. 10 (b)–(f)). The maximum errors on the roof are around 100%, 92%, 33%, 33%, 31% and 33% for f_{max} values of 10, 8, 4, 3, 2, and 1 respectively. Whereas the errors are far higher in all the six cases on the windward and leeward sides, the errors are reduced somewhat for lower f_{max} .

The maximum errors on the windward and leeward side for the six cases in the order of decreasing f_{max} are 600%–200%. Therefore, the f_{LES} cutoff issues on the C_{pmin} can be seen. According to Fig. 10(a)–10(c), a dramatic reduction in error on the roof and side walls is observed due to f_{LES} issue or the error in transporting high-frequency velocities that cannot be transported by the given grid spacing of h. The changes are not noticed from Fig. 10(c) to Fig. (f). The suggestion of 4 points to represent the shortest wave or for f_{LES} by Ferziger and Peric [18] is reasonable in this case.

The maximum pressure coefficients C_{pmax} are also compared in Fig. 11(a)–(f) with WT and field measurements using H/16 grid for the same f_{max} . The effect of $f_{max} > f_{LES}$ has the same trend as before. The CFD C_{pmax} were approaching the WT and field measurements on all sides as the f_{max} decreases up to four. For $f_{max} = 4$ or less, the CFD C_{pmax} has high errors (more than 200%) on the roof with respect to WT measurements. Whereas in Fig. 10, the roof pressures are much closer (around 20% error) compared to WT measurements.

As it can be seen, peak pressure on the building gets high errors due to spurious pressure. In CDRFG methods, there is not any control on initializing the maximum wavenumber and it is chosen randomly and

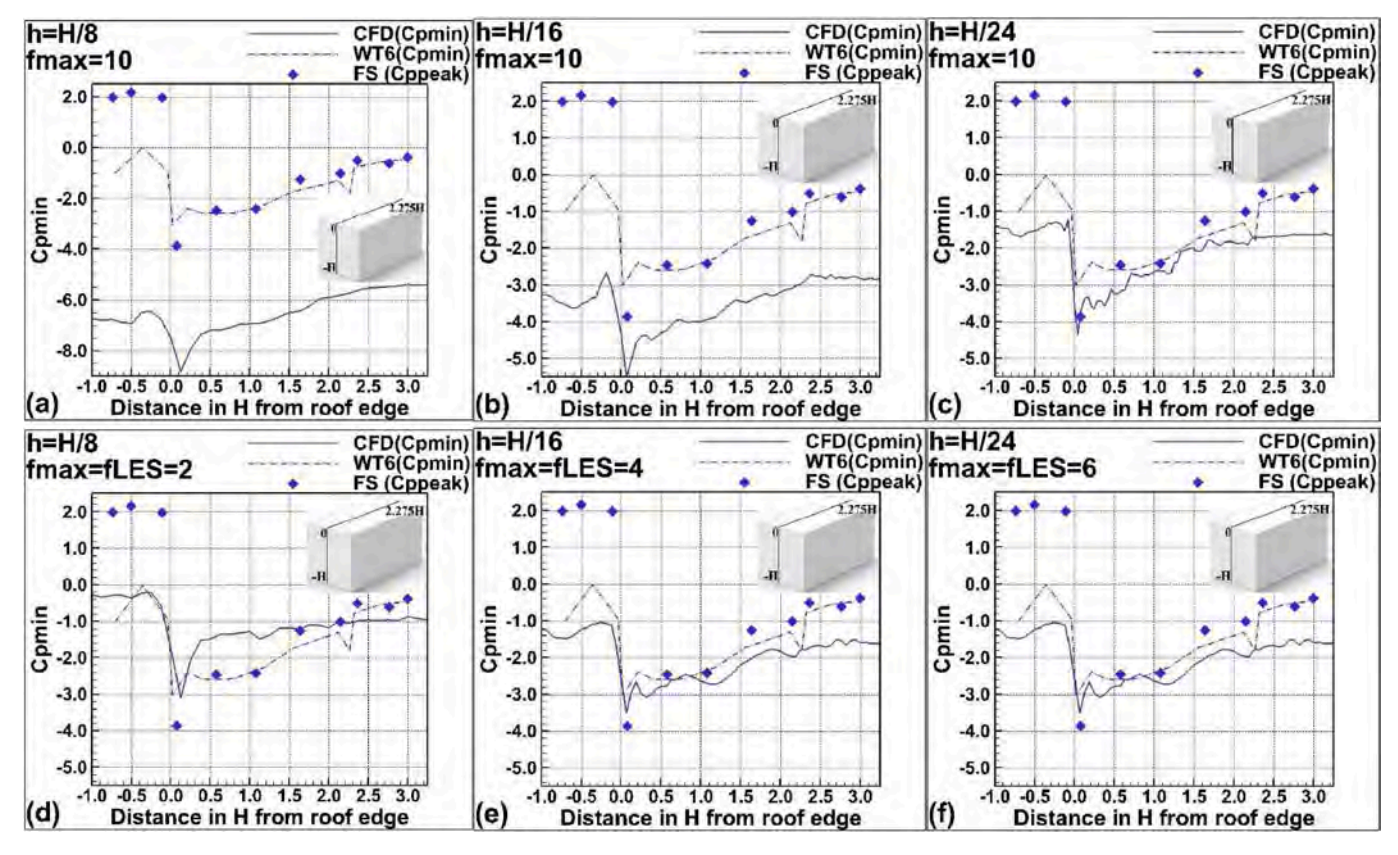


Fig. 8. Grid convergence study for minimum pressure coefficients for (a) h = H/8 and $f_{max} = 10$, (b) h = H/16 and $f_{max} = 10$, (c) h = H/24 and $f_{max} = 10$, (d) h = H/8 and $f_{max} = f_{LES} = 2$, (e) h = H/16 and $f_{max} = f_{LES} = 4$, and (f) h = H/24 and $f_{max} = f_{LES} = 6$.

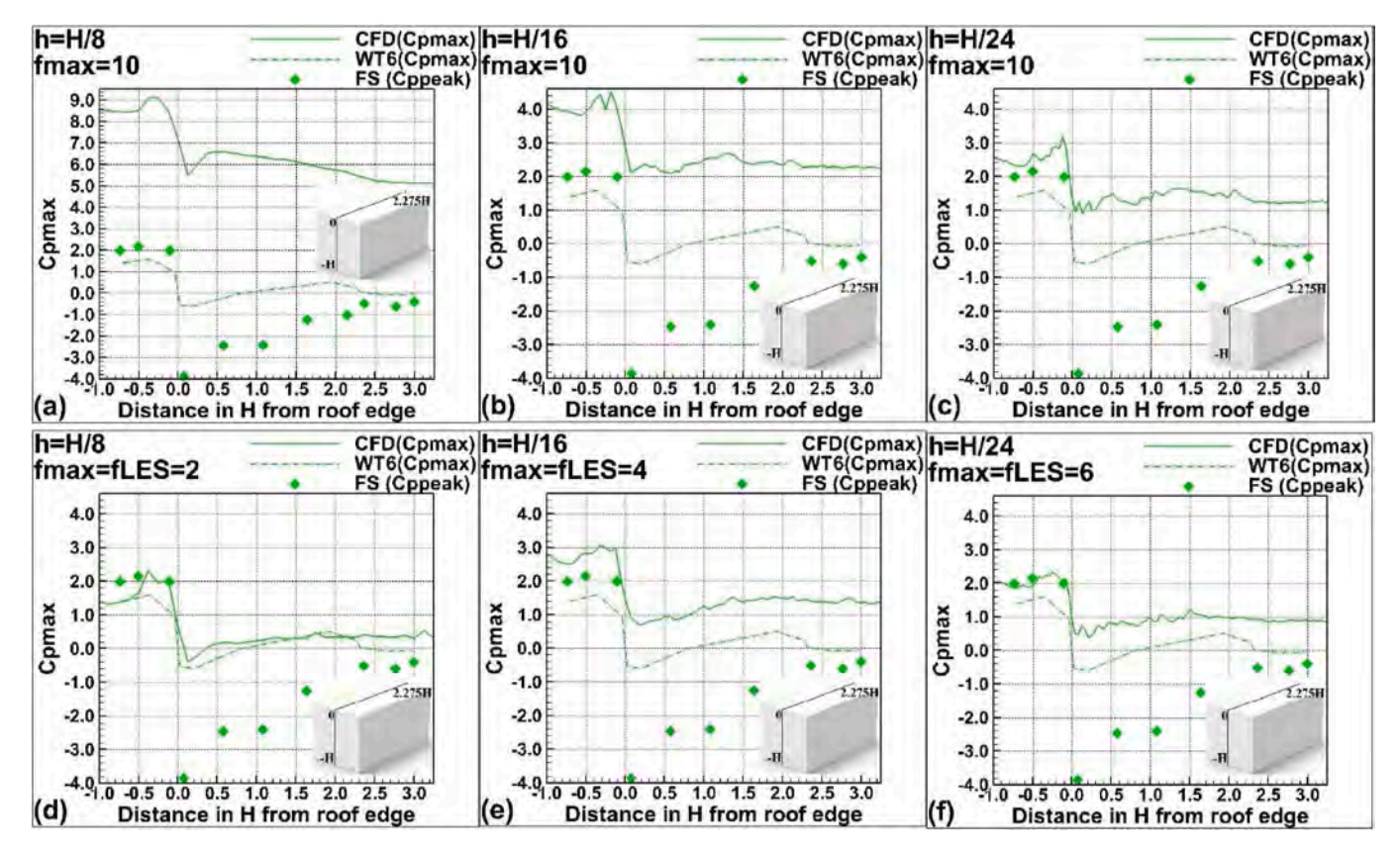


Fig. 9. Grid convergence study for maximum pressure coefficients for (a) h = H/8 and $f_{max} = 10$, (b) h = H/16 and $f_{max} = 10$, (c) h = H/24 and $f_{max} = 10$, (d) h = H/8 and $f_{max} = f_{LES} = 2$, (e) h = H/16 and $f_{max} = f_{LES} = 4$, and (f) h = H/24 and $f_{max} = f_{LES} = 6$.

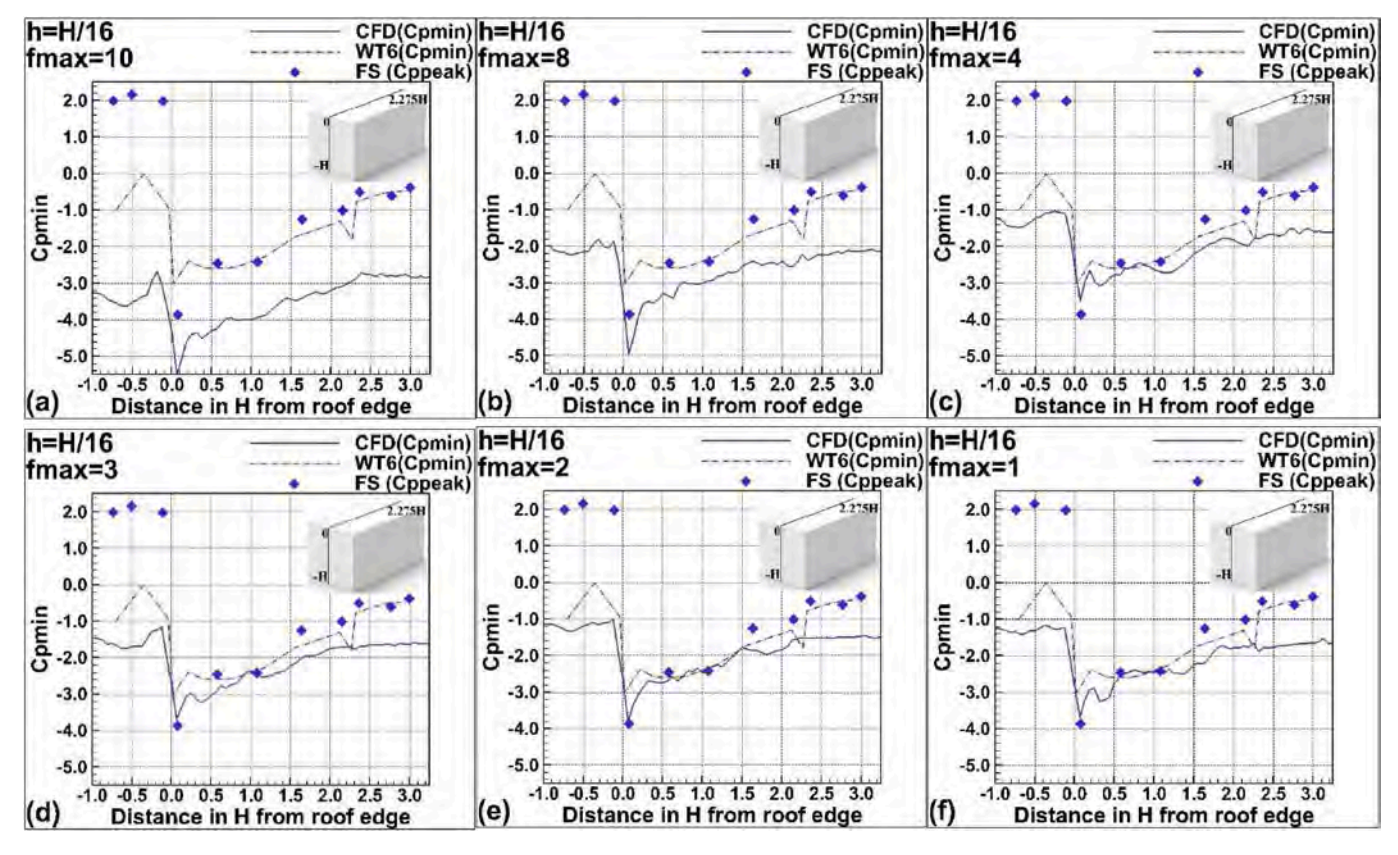


Fig. 10. Minimum pressure coefficients for various f_{max} using H/16 grid spacing (a) $f_{max} = 10$, (b) $f_{max} = 8$, (c) $f_{max} = 4$, (d) $f_{max} = 3$, (e) $f_{max} = 2$, and (f) $f_{max} = 1$.

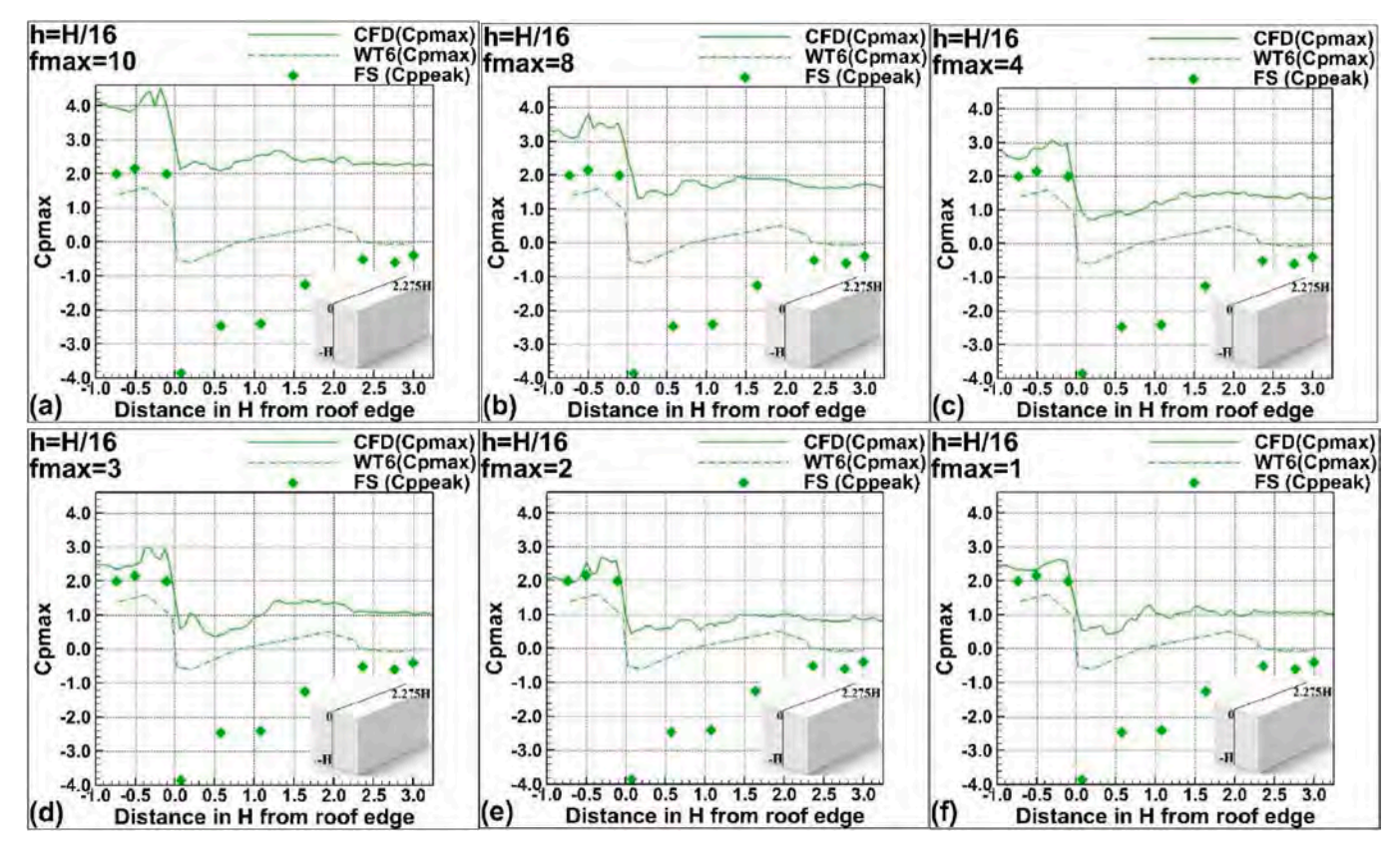


Fig. 11. Maximum pressure coefficients for various f_{max} using H/16 (a) $f_{max} = 10$, (b) $f_{max} = 8$, (c) $f_{max} = 4$, (d) $f_{max} = 3$, (e) $f_{max} = 2$, and (f) $f_{max} = 1$.

then corrected with forcing continuity equations. To illustrate this, the maximum wavenumber can be carried by the grid, the CDRFG wavenumber, and general methods wavenumber are provided below:

These wavenumbers are calculated for the grid spacing size of H/16 and $f_{max}=f_{LES}=4$, in the building height of H=3.96 m, and $U_{\rm H}=7.66$ m/s.

- 1. For the CDRFG method, the equivalent wavenumber is $k_j^{m,n} = k_j^{m,n} f_m \gamma C_j / U_{ave}$ from Eqn. (4) (i.e., the CDRFG method's velocity equation). Hence, the maximum dimensional wavenumber can be calculated as $k_{d_{CDRFG}} = 65.6$ (1/m) in the direction X (driven from CDFRG output). Subsequently, the maximum nondimensional wavenumber is $k_{n_{CDRFG}} = 260$.
- 2. In general, for other methods, the relation between wavenumber and frequency in the many RFG methods is $k_{d_G}=2\pi n/U_{ave}$. Hence, the maximum dimensional wavenumber is $k_{d_G}=2\pi n_{max}/U_H=6.55$ (1/m) in the direction X. Subsequently, the maximum nondimensional wavenumber is $k_{n_G}=25.97$.
- 3. The dimensional LES wavenumber is $k_{d_{LES}}=2\pi/(4h)$ (1/m) in the direction X as the maximum wavelength is L=4h for LES. Subsequently, the nondimensional LES wavenumber is $k_{n_{LES}}=2\pi H/(4h)=25.12$.

As it can be seen, using $f_{max} = f_{LES}$ leads to having a wavenumber less than k_{LES} in methods that considered the general relation between frequency and wavenumber. Whereas, in the CDRFG, using $f_{max} = f_{LES}$ does not lead to wavenumber being less than k_{LES} and it led to existing peak pressure errors even for $f_{max} = f_{LES}$.

6.2.3. Comparison of mean pressure coefficients for various f_{max} with WT The mean pressure coefficients C_p are calculated from 10 time units to 100 time units at each point along the centerline of the TTU building. The mean C_p values are comparable with WT6 as shown in Fig. 12(a)–(f)

for the six f_{max} considered. Only minimal differences from one plot to another are noticed. The maximum error of 20% between WT and CFD is noticed at the windward roof edge, and in other places, the errors are less than this value. This discrepancy could be due to the particular inflow turbulence method used. This also can be easily seen that the mean pressure coefficient does not show the differences which exist and have been shown with peak pressure results.

6.3. Suggestion to use $f_{max} = f_{LES}$ in synthetic inflow methods

The inlet velocity spectrums, as well as the corresponding velocity spectrums at the windward edge of the building without the building, are shown in Fig. 12 at the building height of $f_{max} = 2$, 4, and 10 as a sample. The targeted f_{max} is realized at the inflow as shown in Fig. 13(a)– 13(c). A dashed vertical line is placed in each figure to show the f_{max} point. According to Fig. 12(a) for f_{max} of 10, the high-frequency amplitude or energy is cut off beyond $f_{max} = f_{LES} = 4$ at the building location due to the grid resolution effect. Whereas there is a reasonable correlation between the inlet and building location spectrum in Fig. 13(b) and (c) when the f_{LES} is less than or equal to $f_{LES} = 4$. However, for all cases the oversampled further than the targeted f_{max} is observed. This $f_{max} = 2$ is for the smallest wavelength of 8h. Generally, it is proposed to use more than 10 points for a wave using FDM to have less error but this can take more computer time. However, as peak pressure results error for smaller f_{max} than 4 roughly equal to the peak pressure results for f_{max} of 4, hence, choosing f_{max} of 4 (i.e., L of 4h) is reasonable to avoid computational

Overall observations from this analysis are as follows:

1. As per the LES theory, for a given grid spacing h, the f_{max} to be used in the inflow spectrum is f_{grid} (4 when L=4h for h=H/16) and this is called f_{LES} . The high frequencies beyond this value are modeled by subgrid-scale modeling like the Smograinsky model. If this is violated

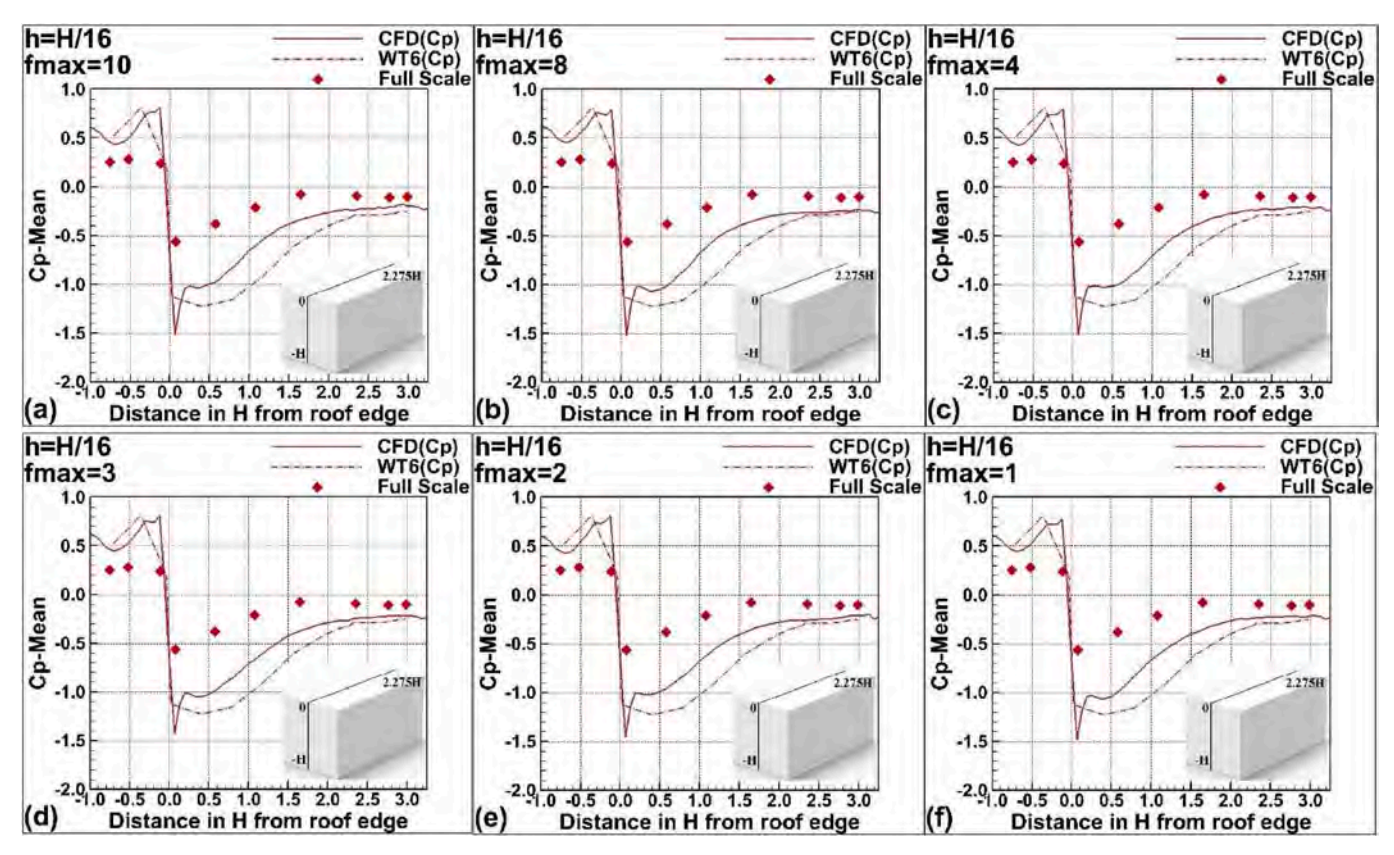


Fig. 12. Mean pressure coefficients for various f_{max} using H/16 grid spacing (a) $f_{max} = 10$, (b) $f_{max} = 8$, (c) $f_{max} = 4$, (d) $f_{max} = 3$, (e) $f_{max} = 2$, and (f) $f_{max} = 1$.

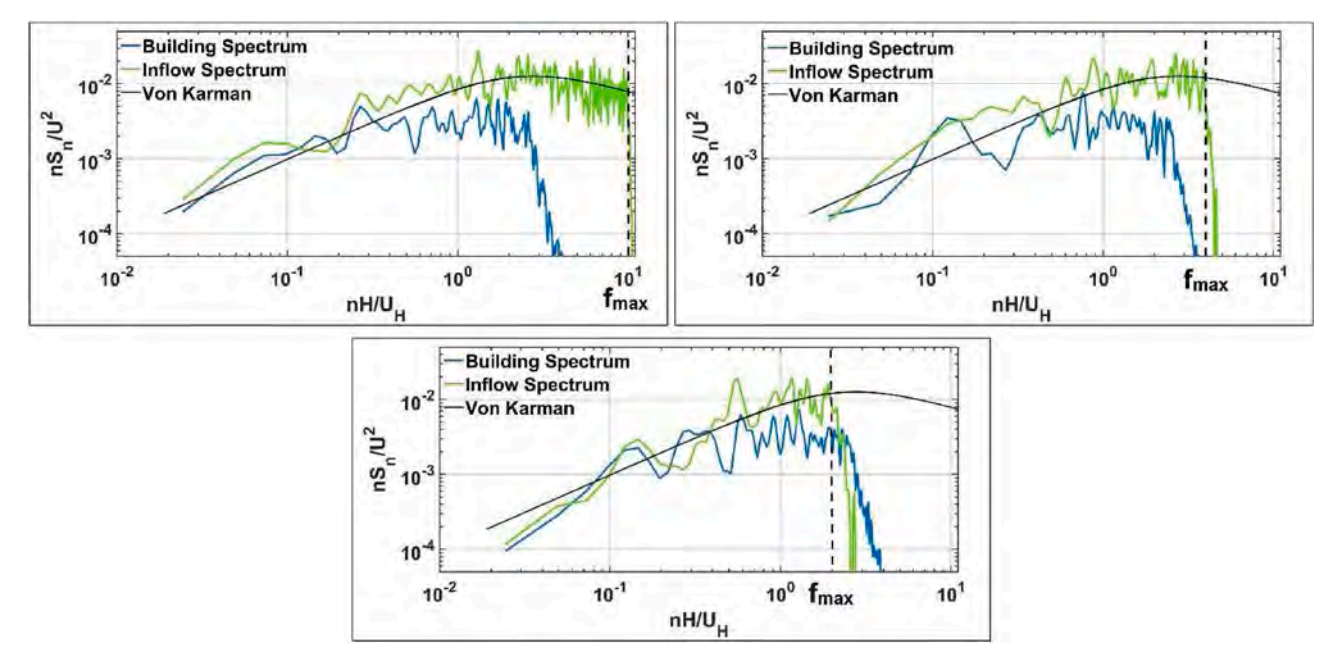


Fig. 13. Velocity spectrum at the inlet and building location without building for various f_{max} using H/16 grid (a) $f_{max} = 10$ (b) $f_{max} = 4$ and (c) $f_{max} = 2$.

there are spurious pressures. This is illustrated using velocity and pressure plots at the building location without building computations.

- 2. Due to spurious pressure, the peak pressure on the building gets high errors and this is not illustrated in the past.
- 3. Thus the $f_{max} > f_{LES}$ effect on peak pressure is not been properly understood from the CFD point of view in the past. This is illustrated systematically by considering different f_{max} .
- 4. From our calculations, it is found that even for $f_{max} = 4$, the peak pressure has some error for H/16 grid. This is because frequency cutoff does not lead to wavenumber cutoff in the CDRFG method.
- 5. The final conclusion is, the peak pressures are affected by f_{max} and one has to be careful in making the proper choice of f_{max} for a given grid size.

Procedure for computation of inflow turbulence using synthetic inflow turbulence method:

- 1. Get the f_{maxe} and f_{mine} from the field or wind tunnel experiment.
- 2. Decide on the largest grid spacing h to be used for the CFD modeling. This depends upon the computer storage and time available. Using this h calculate $f_{grid} = H/L_{min}$ where $L_{min} = 4h$. Then keep $f_{max} = f_{LES} = f_{grid} = H/L_{min}$ in the inflow turbulence generator
- 3. The smallest frequency f_{min} is kept as f_{mine} .
- 4. Using these parameters calculate the inflow turbulence.

7. Conclusions

The following conclusions are made by comparing the CFD peak pressures with 1:6 scale TTU wind tunnel peak pressures for different grid spacing.

- 1. The largest grid spacing h in the computational domain determines the highest frequency of the velocity fluctuations transported by the grid (f_{grid}) from the inflow turbulence. In the LES computation, the suggested highest frequency transported in the flow using the finite difference method (FDM) is $f_{LES} = f_{grid} = H/4 \ h$ where 4 h is the smallest wavelength resolved by the grid.
- 2. If $f_{max} > f_{LES}$ velocity spectrum is considered at the inlet, these velocities introduce spurious pressures at the building locations.

3. Spurious pressures lead to having high errors in peak pressure results (more than 600% error on the sidewall and 100% on the roof for H/16 grid) on the building. This is illustrated by comparing the CFD pressure with WT measurement for the TTU building. The computed inflow turbulence using the CDRFG method for $f_{max} = f_{LES}$ input cases also has some level of spurious pressures due to k_{LES} violation in the CDRFG method. However, using $f_{max} = f_{LES}$ for all the grid spacing size of H/8, H/16, and H/24 leads to reductions of spurious pressure and improvement of peak pressure results.

Data availability statement

Some or all data, models, or code generated or used during the study are available from the corresponding author by request.

All plotted data.

Credit author statement

Zahra Mansouri: Conceptualization, Software, Formal analysis, Investigation, Data Curation, Writing - Original Draft, Review & Editing, Visualization. Rathinam Panneer Selvam: Conceptualization, Methodology, Software, Resources, Writing - Review & Editing, Supervision, Project administration, Funding acquisition. Arindam Gan Chowdhury: Validation, Resources, Writing - Review & Editing.

Declaration of competing interest

The authors declare the following financial interests/personal relationships which may be considered as potential competing interests: Zahra Mansouri reports was provided by University of Arkansas Fayetteville.

Acknowledgments

Ms. Zahra Mansouri acknowledges the financial support from the James T. Womble Professorship from the University of Arkansas. For this research, wind tunnel data from the NHERI WOW EF were used. The authors acknowledge the help provided by Dr. M. Moravej from Walker Consultants in delivering the wind tunnel data in a way we could use it in this work. The authors also acknowledge Dr. G. Bitsuamlak and his

research group for providing the CDRFG MATLAB code to generate the inflow turbulence.

research group for providing the CDRFG MATLAB code to generate the

Notation

```
The following symbols are used in this paper
          Amplitude of the wave equation
          Mean pressure coefficient
C_p =
         Minimum pressure coefficient
C_{pmax} = Maximum pressure coefficient
         Non-dimensional time step
dt =
dT =
         Dimensional time step
f =
         Non-dimensional frequency = nH/U_H = H/L
f_{LES} =
         Maximum frequency cutoff for LES
f_{grid} =
         Maximum frequency transported by the grid spacing h using FDM
```

 $f_{max} = Maximum$ frequency provided for MATLAB code for inflow computation $f_{min} = Minimum$ frequency provided for MATLAB code for inflow computation $f_{maxe} = Maximum$ frequency from the field or WT velocity spectrum

 $f_{maxe} = Maximum$ frequency from the field or WT velocity spectrum $f_{mine} = Minimum$ frequency from the field or WT velocity spectrum H = Building height

 $h = Maximum \ grid \ spacing$ $I_u = Turbulence \ intensity \ in \ x \ direction$ $I_v = Turbulence \ intensity \ in \ y \ direction$ $I_w = Turbulence \ intensity \ in \ z \ direction$ $k_m = Wavenumber \ in \ the \ many \ RFG \ methods$

 $k_j^{m,n}$ = Wavenumber in the CDRFG method $k_H^{m,n}$ = Maximum wavenumbers at the building height

 $k_i^{m,n} = \infty$ coordinates of uniformly distributed points on a unit radius sphere that satisfy the divergence-free condition in the CDRFG method

L= Wavelength for a given frequency n $L_{min}=$ Smallest wavelength transported by LES $L_u=$ Turbulence length scale in x direction $L_v=$ Turbulence length scale in y direction $L_w=$ Turbulence length scale in z direction

M = Number of random frequencies in one segment for CDRFG

N = The number of frequency segments for CDRFG

n = Dimensional frequency

 $n_{max} = Maximum$ dimensional frequency $n_{min} = Minimum$ dimensional frequency Re = Reynolds number $= U_H H / \nu$

 $T_{ref} = ext{Reference time}$ $U_{ave} = ext{Average velocity}$

 $U_H =$ Average velocity at building height

 $x_i =$ Real coordinates

 $x_i^m =$ Non-dimensionalized coordinates

 $z_0 =$ Roughness length $\Delta =$ Filter length in LES

 $\lambda = \text{Non-dimensional wavelength } = L/H = U_H/nH$

Appendix A

Details of the Pressure Coefficient Graphs

The pressure results were reported in different plot types explaining in the following to understand the effects of different inflow turbulence conditions on the building peak pressure. The average, maximum, and minimum C_p versus x-distance along the building centerline with the origin on the roof edge (Fig. A.1).

Fig. A.1. The centerline of the building with the origin on the roof edge considering in peak pressure result presentations.

Appendix B

Grid Spacing h and the Wave Frequency (f_{grid}) Transported Using FDM with Less Error Example:

To understand the amount of error involved in transporting a sine wave with wavelength L=2h and 4h, let us transport a sine wave of amplitude A with constant velocity for a computational domain length of 2 L. Thus the number of grid points (*IM*) in the computational domain will be IM=5 for L=2h and IM=9 for L=4h. The governing equation and boundary conditions are:

$$\frac{\partial A}{\partial t} + \frac{\partial A}{\partial x} = 0.0 \text{ with } 0 < x < 2L, \begin{cases} at \ x = 0 \Rightarrow A = \sin\left(-\frac{2\pi t}{L}\right) \\ at \ t = 0 \Rightarrow A = \sin\left(\frac{2\pi x}{L}\right) \end{cases}$$
(B.1)

The exact value of A for any x and t is: $A = \sin[(2\pi/L)(x-t)]$.

Here L is considered to be 1 unit and the computational domain length is considered to be 2. The propagation speed is unit value. The wave equation is approximated by the central difference (CD) method in space and Crank-Nicolson method in time. On the left end at x=0, the sine function is specified in time. By keeping the CFL number to be 0.1, computation is done for 2.25 units of time. In the LES computation, central difference method is used for space approximation because of no numerical dissipation as discussed by Davidson [29]. The upwind schemes have some level of numerical dissipation and that affect the accuracy of the LES computation with inflow turbulence generation. To illustrate this issue, upwind (UW) method with h=L/4 case is also considered for comparison. Even though practical applications of CFD are three-dimensional and in the turbulent flow, computations get more complicated, the one-dimensional problem gives some idea on the issue we are talking about.

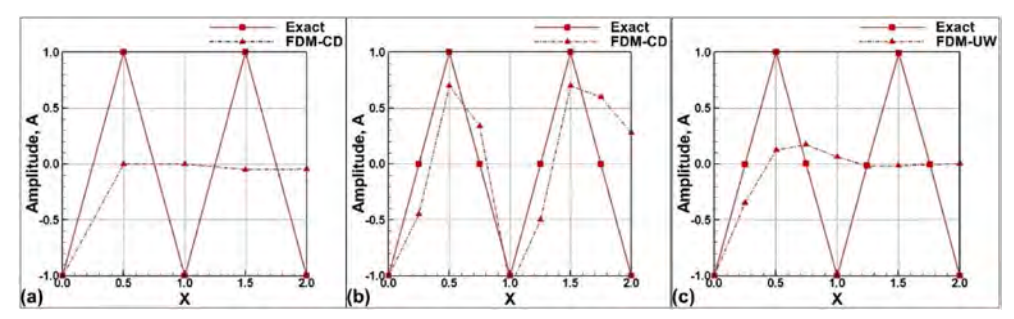


Fig. B.1. Comparison of an exact sine wave transport with the FDM method after 2.25 time units. (a) h = L/2 = 0.5 units using CD method , (b) h = L/4 = 0.25 units using CD method and (c) h = L/4 = 0.25 units using UW method.

From Fig. B.1(a) and (b), one can see that pretty much for h=0.5 (L=2h), the amplitude of the sine wave is close to zero and for h=0.25 (L=4h), one can see the sine wave with some error for CD method. To have a better visualization the exact solution is also plotted for comparison. The performance of UW method for L=4h is shown in Fig. B.1 (c). Because of the diffusive nature of the UW scheme, the amplitude is lost within 2L distance of transport. From this illustration, we can conclude that for a given grid spacing h, a wave-length L=4h or more can be transported, and the corresponding frequency f_{grid} can be calculated using Eq. (1). In calculating f_{grid} one should use the largest grid spacing at the inflow when variable grid spacings are used because any frequency greater than this will be filtered by the grid as shown in Fig. 12 (a) and it is illustrated in section 3.3.

References

- National Weather Service (NWS), National Oceanic and Atmospheric Administration, 2019. https://www.weather.gov.
- [2] J. Woods, Turbulent Effects on Building Pressure Using a Two-Dimensional Finite Element Program, Master Thesis, University of Arkansas, Fayetteville, Arkansas, 2019.
- [3] M.A. Mooneghi, P. Irwin, A.G. Chowdhury, Partial turbulence simulation method for predicting peak wind loads on small structures and building appurtenances, J. Wind Eng. Ind. Aerod. 157 (2016) 47–62.
- [4] R.P. Selvam, Computation of pressures on Texas Tech University building using large eddy simulation, J. Wind Eng. Ind. Aerod. 67 (1997) 647–657.
- [5] A. Keating, U. Piomelli, E. Balaras, H.J. Kaltenbach, A priori and a posteriori tests of inflow conditions for large-eddy simulation, Phys. Fluids 16 (2004) 4696–4712.
- [6] L. Patruno, M. Ricci, On the generation of synthetic divergence-free homogeneous anisotropic turbulence, Comput. Methods Appl. Mech. Eng. 315 (2017) 396–417.

- [7] H. Aboshosha, A. Elshaer, G.T. Bitsuamlak, A. El Damatty, Consistent inflow turbulence generator for LES evaluation of wind-induced responses for tall buildings, J. Wind Eng. Ind. Aerod. 142 (2015) 198–216.
- [8] F. Ding, A. Kareem, J. Wan, Aerodynamic tailoring of structures using computational fluid dynamics, Struct. Eng. Int. 29 (2019) 26–39.
- [9] Y. Yu, Y. Yang, Z. Xie, A new inflow turbulence generator for large eddy simulation evaluation of wind effects on a standard high-rise building, Build. Environ. 138 (2018) 300–313.
- [10] S.J. Daniels, I.P. Castro, Z.T. Xie, Peak loading and surface pressure fluctuations of a tall model building, J. Wind Eng. Ind. Aerod. 120 (2013) 19–28.
- [11] Y. Kim, I.P. Castro, Z.T. Xie, Divergence-free turbulence inflow conditions for large-eddy simulations with incompressible flow solvers, Comput. Fluids 84 (2013) 56-68
- [12] R. Poletto, T. Craft, A. Revell, A new divergence free synthetic eddy method for the reproduction of inlet flow conditions for LES, Flow, Turbul. Combust. 91 (2013) 519–539.
- [13] M. Moravej, Investigating Scale Effects on Analytical Methods of Predicting Peak Wind Loads on Buildings, Ph.D. thesis, FIU., Miami, Florida, 2018.

- [14] T. Rigall, B. Cotté, P. Lafon, Low-noise synthetic turbulence tailored to lateral periodic boundary conditions, Fluids 6 (2021) 193.
- [15] J.S. Haywood, Turbulent Inflow Generation Methods for Large Eddy Simulations, Mississippi State University, 2019.
- [16] L. Lebovitz, Modelling and Time-Resolved Numerical Simulations of Urban Turbulent Wind Flows Around Buildings, Master's Thesis, ETH Zurich, 2017.
- [17] S.A. Orszag, Spectral methods for problems in complex geometrics, in: s), S. V. Parter (Eds.), Numerical Methods for Partial Differential Equations, Academic Press, 1979, pp. 273–305.
- [18] J.H. Ferziger, M. Perić, Computational Methods for Fluid Dynamics, springer, Berlin, 2002.
- [19] A.G. Kravchenko, P. Moin, On the effect of numerical errors in large eddy simulations of turbulent flows, J. Comput. Phys. 131 (1997) 310–322.
- [20] R.P. Selvam, CFD as a tool for assessing wind loading, Bridge Struct. Eng. 47 (2017)
- [21] P. Sagaut, E. Garnier, E. Tromeur, L. Larchevêque, E. Labourasse, Turbulent inflow conditions for LES of supersonic and subsonic wall bounded flows, AIAA (2003) 68, 41st Aerospace Sciences Meeting and Exhibit.
- [22] F.K. Chow, P. Moin, A further study of numerical errors in large-eddy simulation, J. Comput. Phys. 184 (2003) 366–380.
- [23] Z.A. Rana, B. Thornber, D. Drikakis, On the importance of generating accurate turbulent boundary condition for unsteady simulations, J. Turbul. 12 (2011) N35.

- [24] I.W. Kokkinakis, D. Drikakis, K. Ritos, S.M. Spottswood, Direct numerical simulation of supersonic flow and acoustics over a compression ramp, Phys. Fluids 32 (2020), 066107.
- [25] L. Patruno, M. Ricci, A systematic approach to the generation of synthetic turbulence using spectral methods, Comput. Methods Appl. Mech. Eng. 340 (2018) 881–904.
- [26] L. Patruno, S. de Miranda, Unsteady inflow conditions: a variationally based solution to the insurgence of pressure fluctuations, Comput. Methods Appl. Mech. Eng. 363 (2020), 112894.
- [27] Z. Mansouri, R.P. Selvam, A.G. Chowdhury, Performance of Different Inflow Turbulence Methods for Wind Engineering Applications, 2022.
- [28] R.P. Selvam, Computation of flow around Texas Tech building using k ϵ and Kato Launder k ϵ turbulence model, Eng. Struct. 18 (1996) 856–860.
- [29] L. Davidson, Fluid Mechanics, Turbulent Flow and Turbulence Modeling, 2018. Available from:http://www.tfd.chalmers.se/lada/MoF/textbook.html.
- [30] Z.D. Atencio Mojica, Frequency Effect on Peak Pressure Coefficients Using the Narrowband Synthesis Random Flow Generator (NSRFG) Method, Graduate Theses and Dissertations, 2021. Retrieved from, https://scholarworks.uark.edu/etd/4204.
- [31] R. Selvam, Computational Fluid Dynamics for Wind Engineering, Wiley-Blackwell, Chichester, 2022.